

# Estimated contrail frequency and coverage over the contiguous United States from numerical weather prediction analyses and flight track data

DAVID P. DUDA<sup>\*1</sup>, PATRICK MINNIS<sup>1</sup> and RABINDRA PALIKONDA<sup>2</sup>

<sup>1</sup>Science Directorate, NASA Langley Research Center, Hampton, USA

<sup>2</sup>Analytical Services and Materials, Inc., Hampton, USA

(Manuscript received September 9, 2004; in revised form May 19, 2005; accepted May 29, 2005)

## Abstract

Estimates of contrail frequency and coverage over the contiguous United States (CONUS) are developed using hourly meteorological analyses from the Rapid Update Cycle (RUC) numerical weather prediction model and commercial air traffic data for 2 months during 2001. The potential contrail frequency over the CONUS is computed directly from RUC analyses using several modified forms of the classical Appleman criteria for persistent contrail formation. Various schemes for diagnosing contrails from the RUC analyses were tested by first tuning each model to mean satellite estimates of contrail coverage for the domain and then comparing the resulting distributions to those from the satellite retrievals. The most accurate method for forming persistent contrails for both months uses a fourth root relationship between flight lengths and contrail coverage, accounts for contrail overlap and for the dry bias in the humidity profiles, and assumes that contrails can be detected in all cloudiness conditions. The differences between the simulated and satellite-derived contrail amounts are due to errors in the satellite observations, possible diurnally dependent saturation effects, and uncertainties in the numerical weather analysis humidity fields and other input variables. The algorithms developed here are suitable for eventual application to real-time predictions of potential contrail outbreaks. When refined, the methodology could be useful for both contrail mitigation and for contrail-climate effects assessment.

## Zusammenfassung

Es wurden Methoden zur Abschätzung von Kondensstreifenhäufigkeit und -bedeckung über den kontinentalen Vereinigten Staaten von Amerika (CONUS) entwickelt, wozu stündliche meteorologische Analysen des numerischen Wettervorhersagemodells RUC (Rapid Update Cycle) sowie kommerzielle Flugverkehrsdaten aus 2 Monaten des Jahres 2001 verwendet wurden. Die potenzielle Kondensstreifenhäufigkeit über den CONUS wird direkt aus den RUC-Analysen berechnet, und zwar mit Hilfe verschiedener modifizierter Formen des klassischen Appleman-Kriteriums, das die Bildung von persistenten Kondensstreifen beschreibt. Es wurden verschiedene Methoden zur Diagnose von Kondensstreifen getestet, wobei jedes Modell zunächst an den mittleren aus Satellitenbeobachtungen abgeleiteten Kondensstreifenbedeckungsgraden für das Gesamtgebiet kalibriert wurde. Die resultierenden Verteilungen wurden anschließend jeweils mit denen aus Satellitendaten verglichen. Die genaueste Berechnungsmethode der Bildung persistenter Kondensstreifen beinhaltet eine 4.-Wurzelbeziehung zwischen geflogenen Distanzen und Kondensstreifenbedeckung, trägt der Überlappung von Kondensstreifen und dem „dry bias“ in den Feuchteprofilen Rechnung und enthält die Annahme, dass Kondensstreifen unter allen bewölkten Bedingungen detektiert werden können. Die Unterschiede zwischen den simulierten und den aus Satellitendaten abgeleiteten Kondensstreifenbedeckungen sind zurückzuführen auf Fehler in den Satellitenbeobachtungen, mögliche tageszeitabhängige Sättigungseffekte sowie Unsicherheiten in Feuchtefeldern und anderen Eingabegrößen aus der numerischen Wettervorhersage. Die hier entwickelten Algorithmen eignen sich zur zukünftigen Anwendung auf Echtzeit-Vorhersagen der potenziellen Kondensstreifenbildung. In verbesserter Form könnte die Methode sowohl zur Entwicklung von Strategien zur Kondensstreifenvermeidung als auch zu einer genaueren Abschätzung der Klimawirksamkeit von Kondensstreifen beitragen.

## 1 Introduction

Contrails can affect the global atmospheric radiation budget by increasing planetary albedo and reducing infrared emission to space. Our current knowledge of the magnitude of these effects is extremely uncertain. MINNIS et al. (1999) estimated the global mean radiative

forcing by linear contrails to be on the order of  $20 \text{ mW m}^{-2}$ , while more recent estimates show a trend toward lower values of radiative forcing. PONATER et al. (2002) simulated contrail formation within a general circulation model (GCM), and computed a global mean linear contrail forcing of only  $0.2 \text{ mW m}^{-2}$ . MARQUART and MAYER (2002) showed that the results from PONATER et al. underestimate the longwave radiative forcing of contrails by more than a factor of two due to the way the GCM defines cloud overlap and cloud emissivity.

\*Corresponding author: David P. Duda, NASA, Langley Research Center, Mail Stop 420, Hampton, VA 23681-2199, USA, e-mail: d.p.duda@larc.nasa.gov

MYHRE and STORDAL (2001) estimated global radiative forcing by linear contrails using the global contrail coverage data of SAUSEN et al. (1998) and a sophisticated radiative transfer model. MYHRE and STORDAL (2001) derived a global mean forcing of  $10 \text{ mW m}^{-2}$  and emphasized that the forcing was sensitive to the time of day that the contrails form. MARQUART et al. (2003) computed the current and future global linear contrail forcing using an improved version of the PONATER et al GCM and determined a current global net contrail forcing of  $3.5 \text{ mW m}^{-2}$ .

Global radiative forcing by line-shaped contrails is difficult to estimate since it depends on several poorly known factors including the global mean contrail coverage. Current theoretical estimates of global contrail coverage (SAUSEN et al., 1998; PONATER et al., 2002; MARQUART et al., 2003) are tuned to early values of linear contrail coverage determined visually from infrared satellite imagery over the North Atlantic and central Europe (BAKAN et al., 1994). The estimates differ based on the parameterization used to diagnose contrails and the meteorological data employed to determine the ambient conditions. Contrail coverage recently derived over those same areas using an objective detection algorithm (MANNSTEIN et al., 1999; MEYER et al., 2002) are significantly smaller than those given by BAKAN et al. (1994). A comparison of the calculated linear contrail coverage of SAUSEN et al. (1998) with those from analyses of Advanced Very High Resolution Radiometer (AVHRR) data taken over the contiguous United States of America (USA) (PALIKONDA et al., 1999) and the northeastern Pacific (MINNIS et al., 2005A) show that they are similar in overall magnitude, but differ in spatial distribution. Contrail coverage over the contiguous United States (CONUS) during 2001, however, differs significantly from the theoretical estimates in both magnitude and distribution (PALIKONDA et al., 2005). These results illustrate the current uncertainty in linear contrail coverage estimation, a key component in the determination of contrail climate effects.

Development of reliable methods for diagnosing persistent contrails and their physical and radiative properties from numerical weather analyses is essential for predicting future contrail climate impacts. Because air traffic is expected to grow by 2 to 5 % annually (MINNIS et al. 1999), it is important to estimate both the amount and location of contrail coverage accurately. As another step in addressing this concern, actual flight data and coincident meteorological data are used in this paper to estimate contrail coverage over the CONUS for two months using a variety of diagnosis schemes. The estimates are compared with satellite retrievals of contrail coverage based on an objective contrail detection algorithm to determine the most accurate contrail formation scheme and to identify the deficiencies in the methodology and input that need further improvement.

It is important to note that this study (and previous studies) considers only coverage from linear contrails, and the radiative forcing estimates from line-shaped contrails represent the minimum impact of these clouds on climate. Linear contrails sometimes spread into cirrus-like cloudiness that is indistinguishable from natural cirrus (MINNIS et al., 1998). BOUCHER (1999) showed that cirrus clouds increased in occurrence and coverage in the main air-traffic flight corridors between 1982 and 1991, and argued that the increases were due at least in part to aviation effects. MINNIS et al. (2004) estimated the maximum radiative impact of contrail cirrus by assuming that long-term trends in cirrus coverage were due entirely to air traffic in areas where humidity was relatively constant. MINNIS et al. estimate that the maximum contrail cirrus global radiative forcing is between 6 and  $25 \text{ mW m}^{-2}$ , depending on uncertainties in contrail properties.

## 2 Data

### 2.1 Air traffic data

A commercial air traffic database compiled by GARBER et al. (2005) was used to specify air traffic density over the CONUS during September and November 2001. The database was purchased from FlyteComm, Inc., and consists of readings of aircraft (flight number, aircraft type), position (latitude, longitude, altitude), heading, destination and origination locations, speed, and departure and arrival times. These reports were updated every minute for all air traffic within range of the land-based air traffic radars, and every  $10^\circ$  of longitude (approximately 30 minutes) for transoceanic flights that are out of the radar range. FlyteComm ingests the real-time feed from the USA Federal Aviation Administration (FAA) database and reformats it for commercial use. The FAA database includes, at a minimum, all USA Instrument Flight Rules (IFR) flights for which it is responsible (i.e., non-military), all IFR flights monitored by the Transport Canada Aviation Group, all IFR air traffic within several hundred miles of the USA borders, and all transoceanic IFR air traffic that originates or terminates in Canada or the USA. Although the database does not include military flights, it contains most of the air traffic over the CONUS. The FlyteComm data were downloaded every 5 minutes to a local computer hard drive. Daily data files, constructed of all flight reports within a 24-hour period, were sorted by flight number and sub-sorted in turn by departure airport, arrival airport, and time. Data were qualified by eliminating reports that represented pending flights, had an altitude below 25 kft (7.6 km) or above 49.2 kft (15 km), had a location outside the analysis domain ( $20^\circ\text{N}$ – $50^\circ\text{N}$  and  $60^\circ\text{W}$ – $135^\circ\text{W}$ ), or exactly duplicated another line. Air traffic densities were tabulated in terms of cumulative flight path lengths per  $1^\circ \times 1^\circ$  region at a vertical resolution of 1 km between 7 and 15 km in time steps of one hour.

## 2.2 Meteorological and satellite data

Atmospheric profiles of temperature and humidity were derived from the 40-km resolution, 1-hourly Rapid Update Cycle (RUC) analyses (BENJAMIN et al., 2004) in 25-hPa intervals from 400 hPa to 150 hPa. The RUC data were linearly interpolated at each pressure level into a  $1^\circ \times 1^\circ$  grid that extends from  $25^\circ\text{N}$  to  $56^\circ\text{N}$  and from  $129^\circ\text{W}$  to  $67^\circ\text{W}$ . Because the domains of the flight track data and meteorological data do not coincide, the analysis region for this study is the intersection of both domains (i.e.,  $25^\circ\text{N}$ – $50^\circ\text{N}$  and  $129^\circ\text{W}$ – $67^\circ\text{W}$ ).

The RUC analyses at 00 UTC and 12 UTC were not used in this study to insure that the humidity fields for each hour were consistent. Before February 2002, a “quick-look” version of the 00 UTC and 12 UTC analyses was collected that did not include all available radiosonde data. Both analyses are noticeably drier in the upper troposphere than the analyses from other hours.

The satellite datasets for deriving contrail and cloud coverage consist of infrared radiances from the Sun-synchronous NOAA-16 AVHRR 1-km imager (10.8 and  $12.0\ \mu\text{m}$ ) and multi-spectral 1-km data from the Moderate Resolution Imaging Spectroradiometer (MODIS) on the Terra satellite (BARNES et al., 1998). Linear contrail features were detected from the AVHRR data using the automated detection algorithm of MANNSTEIN et al., (1999). This objective method uses a combination of the brightness temperature difference between the 10.8 and  $12.0\ \mu\text{m}$  channels, the  $12.0\ \mu\text{m}$  brightness temperature data, and a set of line filters to detect line-shaped contrails. The multi-spectral MODIS data were used to determine areas of cloudiness that may obscure contrail detection (MINNIS et al., 2002).

## 3 Method

Persistent contrail formation was computed according to the classical criteria of APPLEMAN (1953) using the RUC profiles of temperature and humidity. The contrail formation algorithm follows SCHRADER (1997), modified with the aircraft propulsion efficiency parameter of BUSEN and SCHUMANN (1995). The mean value of the propulsion efficiency assumed for the present commercial fleet was 0.30 (SAUSEN et al., 1998). The saturation vapor pressure coefficients of ALDUCHOV and ESKRIDGE (1996) [AERW(50,–80) and AERWi(0,–80)] were used to compute saturation vapor pressure over water and ice.

According to classical contrail formation theory, contrails can persist when the ambient air is supersaturated with respect to ice (that is, the environmental RHI is greater than 100 %), but not with respect to water. In SAUSEN et al. (1998), the use of ECMWF reanalysis data required a contrail parameterization to compute persistent contrail coverage since the RHI values in the ECMWF model rarely exceed 100 %. The RUC model

contains a sophisticated cloud and moisture scheme that allows for ice-supersaturation. Assuming that the RUC upper tropospheric moisture variables are accurate, we can follow a much simpler statistical evaluation of potential persistent contrail frequency. For each  $1^\circ \times 1^\circ$  grid box where the criteria for persistent contrails occur at any level from 400 hPa to 150 hPa, a persistence indicator is given a value of 1 for each hourly analysis. The indicator equals zero when none of the levels satisfies the persistence criteria. The potential contrail frequency (PCF) over a time period becomes simply the frequency of occurrence of the hourly persistence indicator at a particular location. DUDA et al. (2004) demonstrated that the RUC often underestimates upper tropospheric humidity by showing that persistent contrails developed in regions where the RUC computed an RHI of only 85 %. Additional simulations (not shown here) indicate that although adjusting the contrail formation criteria to a lower RHI increases contrail coverage, the change does not significantly affect the overall pattern of the CONUS contrail coverage.

As an initial quality check, the RUC-based potential contrail frequencies were compared to daily estimates of CONUS contrail coverage based on visual inspection of 4-km imagery from the eighth Geostationary Operational Environmental Satellite (GOES-8). The  $10.8\ \mu\text{m}$  minus  $12.0\ \mu\text{m}$  brightness temperature difference images between 1045 UTC and 0045 UTC were examined for the occurrence of contrails within each state of the CONUS. For each day of the analysis, a persistence indicator value of 1 was given for each state in which at least one contrail appeared. The contrail frequency for each state is the percentage of the total analyzed days with contrail occurrence. The monthly mean contrail frequency for all states in the CONUS region was defined as the observation index. The comparison is shown in Figure 1 for the period between January 2001 and April 2003.

As expected, the PCFs computed from the RUC model are higher than the observation index since the RUC-derived frequencies measure the maximum potential for persistent contrail formation while the index is based on visual observations of contrails. The observation index is affected by air traffic patterns and the presence of obscuring cloudiness. Because the observation index is based on observations of 4-km resolution data, it will likely miss narrow contrails. Despite these differences, it is anticipated that the PCF and observation index should have similar trends in magnitude since both are based on the underlying synoptic weather patterns of upper-tropospheric temperature and humidity. The potential contrail frequencies and the observation indices have similar seasonal cycles except after April 2002 when the data from a new version of the RUC model (RUC20) were used. The apparent correlation between the model contrail frequency and the GOES-8 index abruptly disappears at that point. The divergence

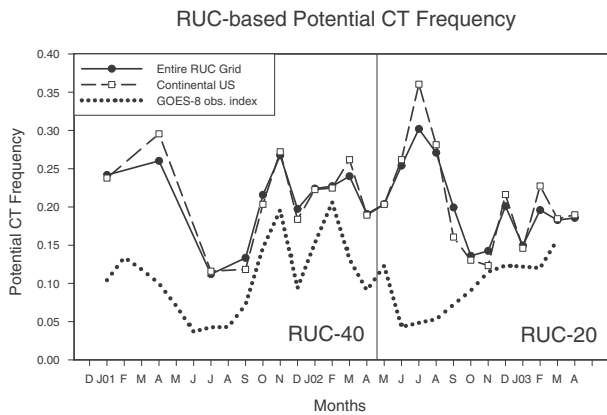
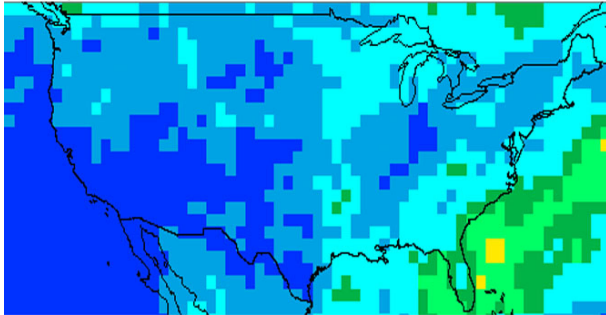


**Figure 1:** Time series of potential contrail frequency computed from RUC analyses between January 2001 and April 2003. The solid line is the frequency computed for all RUC grid points, while the dashed line only includes grid points over the CONUS. The dotted line indicates the GOES-8 observation index.

a) September 2001



b) November 2001

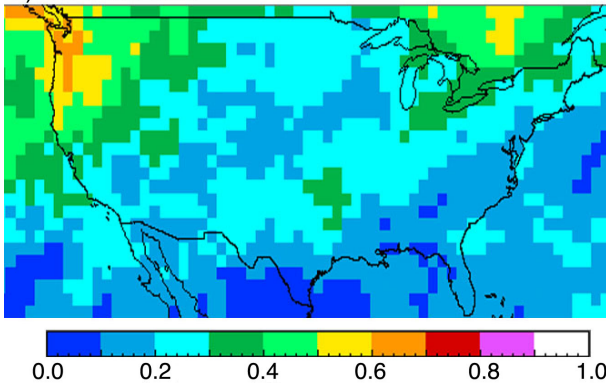


**Figure 2:** (a) Ice-cloud amount computed from Terra MODIS daytime observations during September 2001. (b) Same as (a), but for November 2001.

between PCF and the GOES-8 index during this period is likely the result of changes in the convective parameterization and ice cloud formation model introduced in the newer RUC20 model. The older RUC40 model allowed the development of relatively large, realistic supersaturations while the RUC20 set the RHI = 100 % wherever the model diagnosed a cloud and converted the remaining regions to RHI = 80 % resulting in less realistic probability distributions of RHI. Because

of the correlation between PCF and the GOES-8 index, only RUC40 data are considered hereafter. Due to the limited availability of satellite-derived contrail coverage analyses (PALIKONDA et al., 2005), only two months of RUC40 data (September and November 2001) were used to compute contrail coverages that could be compared to the available satellite data.

To compute the actual contrail coverage, the PCF must be multiplied by the air traffic density. For an initial estimate, (hereafter called scenario A), we will assume that the air traffic density is sparse enough to relate the contrail fractional coverage to the total air travel linearly. The unknown quantity is the mean fractional persistent contrail coverage,  $c_{flt}$ , that results from each kilometer of air travel within a given area. In this study  $c_{flt}$  was tuned to match the CONUS mean contrail coverage from monthly satellite-based contrail coverage estimates (PALIKONDA et al., 2005). The value of  $c_{flt}$  for scenario A varied by 19 % between September 2001 ( $3.72 \times 10^{-5}$ ) and November 2001 ( $4.49 \times 10^{-5}$ ). The RHI threshold for contrail formation was set to 100 % throughout the entire model domain. Only satellite-derived contrail coverage actually measured within the CONUS borders was used for the tuning. No overlap of the contrails is assumed in this simple estimate because contrail altitude is not considered. The total persistent contrail coverage ( $c_{sum}$ ) in a grid cell is simply

$$c_{sum} = PCF \times c_{flt} \times n \quad (3.1)$$

where PCF is the potential contrail frequency for the column between 400 and 150 hPa,  $c_{flt}$  is the mean fractional persistent contrail coverage per distance traveled within a grid cell, and  $n$  is the monthly-integrated path length for flights between 400 and 150 hPa within a grid cell. Note that both PCF and  $n$  are integral quantities derived from available hourly RUC data during each month, and that  $c_{flt}$  is a normalization factor that equates the RUC-simulated contrail coverage with the satellite-derived coverage.

To account for the effects of natural cloudiness obscuring the detection of contrails, the persistence indicator used in the computation of PCF in scenario A was set to zero whenever a grid box was more than 50 % covered by clouds. Although this restriction may lead to an underestimation in contrail coverage, we note that contrails that form in regions of substantial overcast will have smaller radiative forcing (and a smaller effect on global climate) than those in mostly clear regions.

Scenario A was set up as the base case using simple assumptions about contrail formation. For example, in high air traffic regions, it is likely that contrail coverage is non-linearly related to air traffic density due to “saturation” effects (i.e. competition for moisture or overlapping of contrails in air traffic corridors may limit the number of linear contrails that are visible by satellite). If a square-root (or fourth root) relation between

**Table 1:** Root-mean-square (RMS) differences between the observed CONUS contrail coverage and several simulated contrail coverages. Simulations are specified by contrail coverage/air traffic relationship (linear/sqrt/4<sup>th</sup> root), RHI threshold (temperature dependent/100/85), vertical resolution (no overlap (1 layer) /overlap (4 layers)), and cloud mask (all cloud/thick cloud/high cloud/no cloud). All RMS differences are in percent.

September 2001					
Simulation	Air traffic relationship	RHI threshold	Cloud overlap, vertical resolution	Cloud mask	RMS difference (%)
A	linear	100	no overlap, 1 layer	all cloud (Figure 5a)	0.403
B1	sqrt	100	no overlap, 1 layer	all cloud	0.360
B2	sqrt	85	overlap, 4 layers	all cloud	0.317
C1	sqrt	100	overlap, 4 layers	all cloud	0.399
C2	sqrt	100	overlap, 4 layers	high cloud	0.363
C3	sqrt	100	overlap, 4 layers	thick cloud	0.351
C4	sqrt	100	overlap, 4 layers	no cloud	0.315
C5	sqrt	100	no overlap, 1 layer	no cloud	0.289
D1	sqrt	temp	overlap, 4 layers	all cloud	0.313
D2	4 <sup>th</sup> root	temp	overlap, 4 layers	all cloud	0.295
D3	sqrt	temp	no overlap, 1 layer	no cloud	0.287
D4	sqrt	temp	overlap, 4 layers	no cloud	0.274
D5	4 <sup>th</sup> root	temp	no overlap, 1 layer	no cloud	0.264
D6	4 <sup>th</sup> root	temp	overlap, 4 layers	no cloud (Figure 5c)	0.255
November 2001					
Simulation	Air traffic relationship	RHI threshold	Cloud overlap, vertical resolution	Cloud mask	RMS difference (%)
A	linear	100	no overlap, 1 layer	all cloud (Figure 6a)	0.933
B1	sqrt	100	no overlap, 1 layer	all cloud	0.775
B2	sqrt	85	overlap, 4 layers	all cloud	0.703
C1	sqrt	100	overlap, 4 layers	all cloud	0.792
C2	sqrt	100	overlap, 4 layers	high cloud	0.753
C3	sqrt	100	overlap, 4 layers	thick cloud	0.750
C4	sqrt	100	overlap, 4 layers	no cloud	0.664
C5	sqrt	100	no overlap, 1 layer	no cloud	0.633
D1	sqrt	temp	overlap, 4 layers	all cloud	0.697
D2	4 <sup>th</sup> root	temp	overlap, 4 layers	all cloud	0.630
D3	sqrt	temp	no overlap, 1 layer	no cloud	0.597
D4	sqrt	temp	overlap, 4 layers	no cloud	0.603
D5	4 <sup>th</sup> root	temp	no overlap, 1 layer	no cloud	0.521
D6	4 <sup>th</sup> root	temp	overlap, 4 layers	no cloud (Figure 6c)	0.540

coverage and air traffic were assumed, the computed contrail coverage would be less dependent on air traffic density (SAUSEN et al., 1998). Also, scenario A does not consider the effects of the temperature dependence of the dry bias in upper tropospheric soundings (MILOSHEVICH et al., 2001) that are likely to influence the RUC analyses (MINNIS et al., 2005B). Several options for cloud masks were tested in an attempt to screen out areas supporting contrails that may be undetectable by satellite. One cloud mask eliminated areas where all cloud coverage exceeded 50 % (all cloud), another removed grid points with optically thick clouds ( $\tau > 5$ ) (thick cloud) and a third masked regions with optically thick and high (cloud tops  $> 5$  km) clouds (high cloud). Finally, scenario A has no height dependence in the calculation of PCF while upper-tropospheric humidity sometimes changes quickly with height.

To account for these factors, several additional scenarios were run by systematically altering options for cloud mask, height dependence, air traffic/contrail coverage relationships, and RHI threshold for persistent

contrail formation (see Table 1). In addition to the simple one-layer option, the flight track and RUC data were binned into four altitude regions (7–9 km, 9–11 km, 11–13 km, and 13–15 km), and contrail coverage was computed for each layer. To calculate the total contrail coverage, the coverage for each layer was summed using the random overlap assumption,

$$c_{sum} = 1 - \prod_{k=1}^4 (1 - c_k), \quad (3.2)$$

where  $c_k$  is the fractional contrail coverage for height level  $k$ . Several RHI threshold options were developed to compute the PCF, including a temperature-dependent RHI threshold. The threshold was set to 100 % for temperatures of  $-40$  C or higher, and decreases linearly with temperature at a rate of 1 %/°C between  $-40$ °C and  $-70$ °C. For temperatures below  $-70$ °C the threshold was 70 %. Finally, some scenarios assumed that the contrail coverage in each layer was proportional to the square root (or fourth root) of the air traffic distance

flown in each grid box. For all scenarios, the  $c_{flt}$  parameter was computed such that the magnitude of the simulated coverage matches the satellite-derived coverage. This normalization factor simplifies the comparison between the simulated and satellite-derived coverages.

The next section presents the potential contrail frequencies simulated for September and November 2001 from the RUC analyses. Simulated contrail coverage derived from the combination of RUC and air traffic data is also shown for the two extremes of the model scenarios. The PCF fields are compared with the ice cloud coverage maps retrieved from Terra measurements, and the simulated contrail coverage fields are compared with the contrail coverage derived from NOAA-16 observations. Section 5 compares several model scenarios, discusses how each model option affects the determination of simulated contrail coverage, analyzes possible model errors and concludes with some suggestions for improving the simulation of contrail coverage.

## 4 Results

### 4.1 Potential contrail frequency

High cloud coverage (cloud tops  $> 5$  km) for September and November 2001 was derived from Terra MODIS multi-spectral observations (MINNIS et al., 2002). Figure 2 shows the distribution of ice-cloud amount, a quantity accounting for most clouds above 5 km, observed around 1030 LT from Terra. The upper troposphere was relatively dry over the CONUS during September as indicated by the small amounts of cirrus coverage. The broad maximum off the Atlantic coast resulted from the passage of a tropical storm. During November, cirrus maxima occurred over southeastern Canada and northwestern CONUS.

Figure 3 presents the potential contrail frequency computed for September and November 2001. RUC analyses were available for only 26 of 30 possible days during each month. For both months, maximum PCF occurred over the northwestern CONUS, where values reach 0.33 in September and 0.50 in November. Another region of high frequency during November is the eastern half of the CONUS centered over the confluence of the Mississippi and Ohio Rivers ( $39^{\circ}\text{N}$ ,  $90^{\circ}\text{W}$ ). The prevailing synoptic-scale weather patterns during each month strongly influence the overall distribution and magnitude of the monthly potential contrail frequency. The mean PCF for grid points over the CONUS was 0.118 in September and increased to 0.272 in November. These amounts are comparable to the 11-year average (0.141) over the US computed by SAUSEN et al. (1998).

Figure 4 shows the PCF computed for both months using only the time periods corresponding to the available afternoon ( $\sim 1430$  LT) overpasses of the NOAA-16 satellite. To approximate the satellite coverage in the calculation of the contrail frequencies, only RUC grid

points within  $12^{\circ}$  of longitude of the sub-satellite point at  $37^{\circ}\text{N}$  were counted during each overpass. Although the mean potential contrail frequencies computed for the CONUS were almost identical to the monthly averages (0.139 for September 2001, 0.270 for November 2001), the distribution of PCF is much more variable in Figure 4 than in Figure 3 due to the limited sample sizes.

The PCFs should be related to the occurrence of natural cirrus clouds because the conditions giving rise to cirrus clouds are similar to those for contrail formation except for the lower RHI contrail formation threshold and the low temperature requirement for contrails. During both months, the ice cloud (Fig. 2) and PCF (Fig. 3) patterns are generally similar with some notable exceptions. The differences between the September and November ice cloud amounts (Fig. 2) over the northwestern CONUS are not consistent with the corresponding differences in the PCFs during both months (Fig. 3). This inconsistency suggests that the RUC estimates of RHI over the northwestern CONUS during September are unusually high. During November, the orientation of the axes of maximum cirrus and PCF over the Ohio River Basin (from  $38^{\circ}\text{N}$ ,  $90^{\circ}\text{W}$  to  $41^{\circ}\text{N}$ ,  $80^{\circ}\text{W}$ ) are very similar, but the PCF maximum is broader with the 30 % contour extending eastward over the southeastern coast while the cirrus coverage decreases over the same areas.

### 4.2 Contrail coverage

To facilitate comparisons between satellite-derived and simulated coverage, Figures 5 and 6 show plots of simulated persistent contrail coverage  $c_{sum}$  and satellite-derived contrail coverage for September and November 2001, respectively. The values of  $c_{sum}$  were computed for two diagnosis schemes, scenario A and scenario D6. The results from the two scenarios are plotted in the panels (a) and (c) for each figure respectively. As stated earlier, scenario A represents the base case with the simplest model options. Scenario D6 represents the scheme with the combination of options that gives the best overall match between the simulations and the satellite-derived results. Scenario D6 assumes that the contrail coverage is proportional to the fourth root of the air traffic density, uses the temperature-dependent RHI threshold and the 4-layer option with cloud overlap, and no cloud mask. The differences between scenarios A and D6 illustrate the effects that the model options have on the spatial distribution of  $c_{sum}$ . The satellite-based CONUS contrail coverage estimates, shown in the (b) panels, use NOAA-16 AVHRR data and an objective contrail detection algorithm (MANNSTEIN et al., 1999) to compute contrail coverage (PALIKONDA et al., 2005).

The simulated coverages for scenario A are heavily influenced by the air traffic density pattern (compare with Fig. 7), and are similar in appearance to SAUSEN et al. (1998), with a maximum in the eastern half of the CONUS, and relatively little coverage in the northern

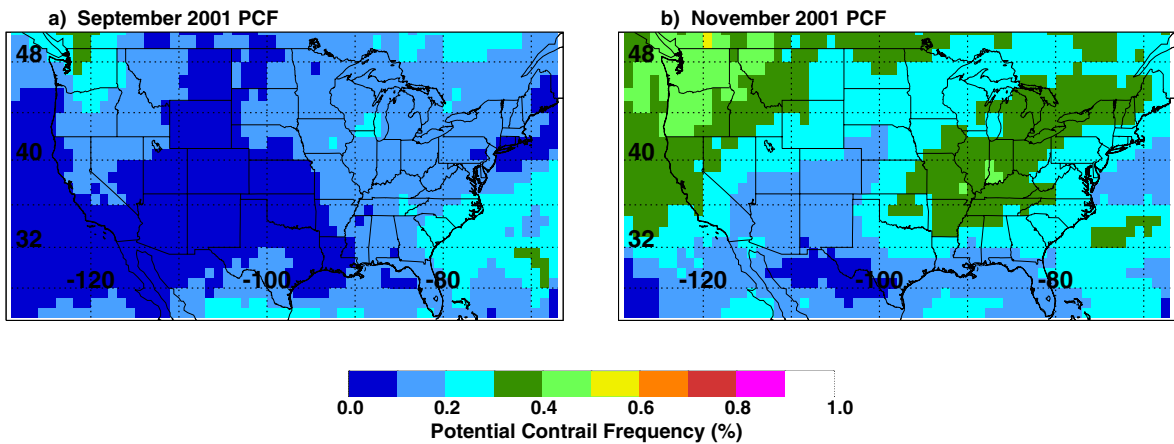


**Figure 3:** (a) Potential persistent contrail frequency computed from RUC analysis for September 2001. (b) Same as (a), but for November 2001.

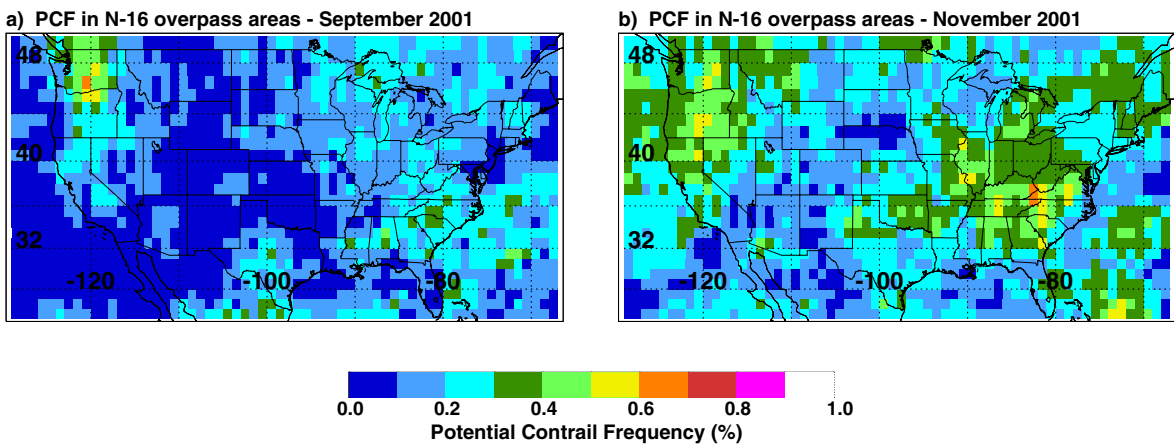


**Figure 4:** (a) Potential persistent contrail frequency computed from RUC analysis during available NOAA-16 afternoon overpass times for September 2001. (b) Same as (a), but for November 2001.

Great Plains (45°N, 100°W and surrounding area). The scenario A coverage for September also has a maximum in the northwestern states that reflects the extremely high PCF in the area computed at the satellite overpass times. The contrail coverage for the CONUS based on the objective satellite analysis is 0.37 % for September 2001 and 1.02 % for November 2001. The satellite results from both months (Figs. 5b and 6b) appear to be similar to the PCF (in other words, the environmental conditions – compare with Fig. 4). The simulated contrail coverages for scenario A (Figs. 5a and 6a) yield larger maxima compared to the coverages for scenario D6 (Figs. 5c and 6c). No relative maxima are evident over the Pacific, Canada, or Mexico due to limited flight information in those areas. The greatest concentration of simulated contrails for scenario D6 appears over the southeastern states and the central Mississippi basin (40°N, 90°W). In scenario D6,  $c_{fl}$  was  $1.16 \cdot 10^{-10}$  for September 2001 and  $1.65 \cdot 10^{-10}$  for November 2001, a relative difference of 35 %.

Although scenario D6 compares better with the satellite-derived coverage than scenario A, many significant differences remain. Figures 8a and 8b show the satellite-derived minus the scenario D6 simulated coverage for September and November 2001 over the CONUS. The simulated September coverage compares well with the satellite-based coverage over much of the eastern third of the US, although the satellite analysis has a maximum over the northeastern states, which may be the result of cirrus streamer contamination due to tropical storms during the month. The simulated coverage also has a strong maximum over Washington and Oregon (46°N, 120°W) that is not seen in the satellite analysis. This maximum results from the extremely large PCF computed for this region at all levels, and may be an artifact of the RUC analysis during this month. The RUC computed unusually high values of upper tropospheric humidity over the northwest during September and over the southeastern CONUS during November during the NOAA-16 overpass times. Figures 5b and 6b have maxima over eastern Montana (47°N, 108°W),

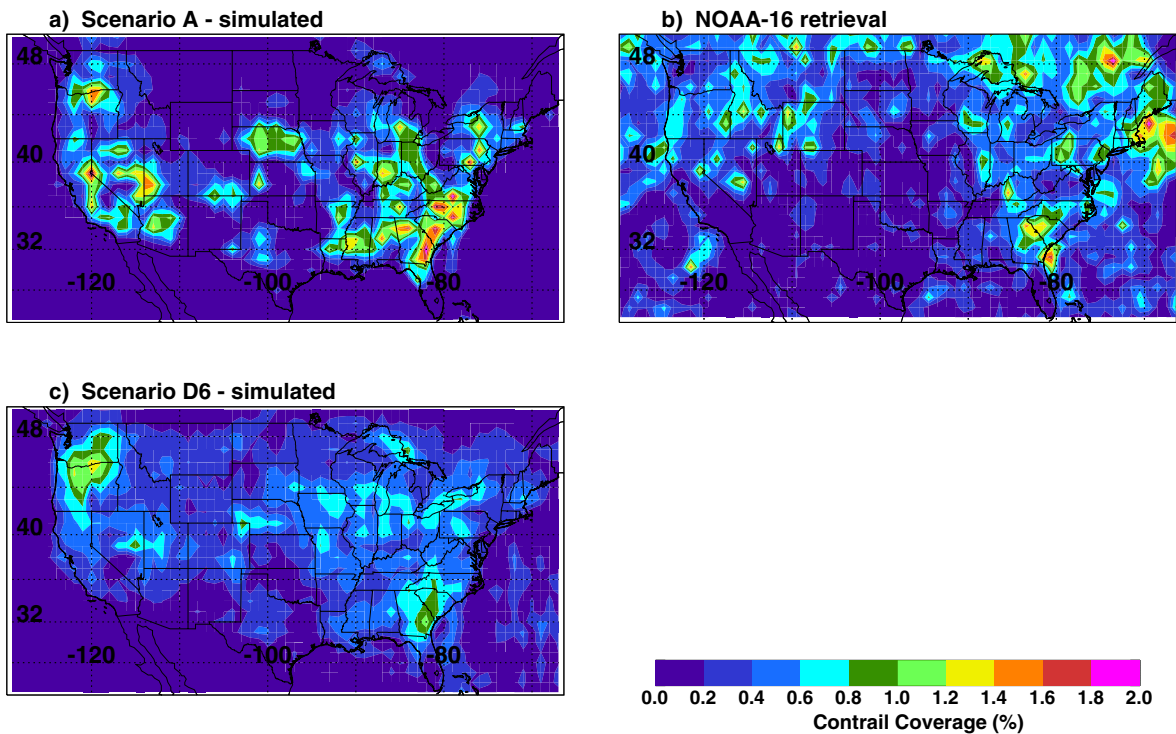


**Figure 5:** (a) Persistent contrail coverage computed for September 2001 in scenario A. Simulation uses a linear relationship between contrail coverage and air traffic density, a constant RHI threshold (100 %), and a high cloud mask. (b) Contrail coverage computed from NOAA-16 afternoon overpasses for September 2001 using an objective analysis. (c) Persistent contrail coverage computed for September 2001 in scenario D6. Simulation uses a fourth root relationship between contrail coverage and air traffic density, a temperature-dependent RHI threshold, and no cloud mask. Contrail coverage is calculated within four equally spaced layers between 7 and 15 km with random overlap between layers.

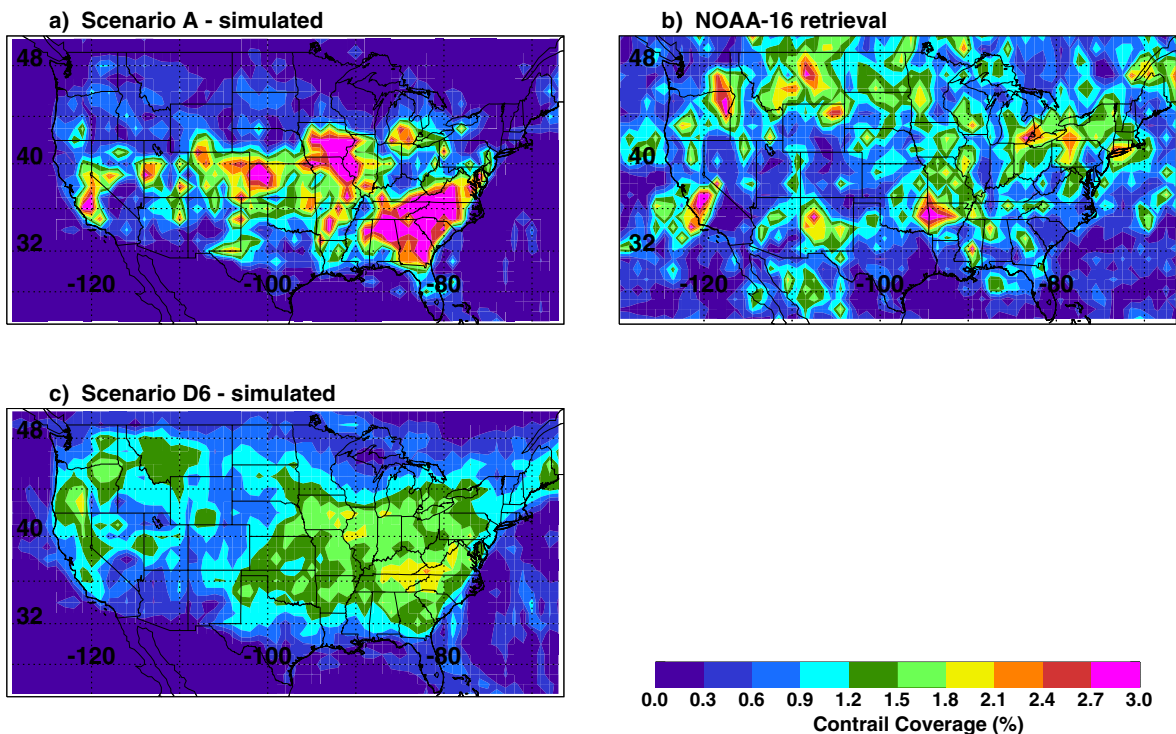


**Figure 6:** Same as Figure 5, but for November 2001.

New York and Pennsylvania ( $42^{\circ}\text{N}$ ,  $77^{\circ}\text{W}$ ), and southern New England ( $43^{\circ}\text{N}$ ,  $69^{\circ}\text{W}$ ) that are not in the simulated results.

Figure 8a shows that the satellite-derived coverage is much higher in a region extending from northern California through the northern Rockies into northern Minnesota (from  $41^{\circ}\text{N}$ ,  $123^{\circ}\text{W}$  to  $49^{\circ}\text{N}$ ,  $95^{\circ}\text{W}$ ). Some of this difference may be due to the presence of military traffic in this region of the CONUS that is not available in the flight track database (BJORNSON, 1992). The simulated coverage may also be lower in these regions due to false contrail detection of cumulus cloud streets and mountain-valley features that are sometimes mistaken as contrails by the automated algorithm (e.g., MINNIS et al., 2005A). A similar difference between the observed and simulated coverage in this region also appears in Figure 8b. Figure 8 shows that the simulated coverage appears to be larger than that observed over the central Plains states (near  $40^{\circ}\text{N}$ ,  $100^{\circ}\text{W}$ ) for both months. This region is in the lee of the Rocky Mountains where negative vertical velocities induced by the topography may suppress the development of contrails in this region. The root mean square (RMS) difference between the satellite-derived coverage and the contrail coverage simulated in scenario D6 was 0.26 % for September and 0.54 % for November 2001.

## 5 Discussion

Several additional scenarios were also tested to determine the effects of each model option on the simulation of contrail coverage. An overall assessment of the results is summarized in Table 1, which lists the root-mean-square (RMS) differences between the satellite-derived and model-simulated contrail coverages for several diagnosis schemes. The inclusion of the fourth root air traffic relationship produced simulated coverages with the smallest RMS differences, although the scenarios using the square root relation were similar in appearance to the fourth-root scenarios. Lowering the RHI threshold to 85 % tended to smooth out the simulated coverage, and to increase the contrail coverage in the eastern CONUS relative to that in the west, but the overall pattern of simulated coverage was similar. The temperature-dependent RHI threshold, however, produced the best overall results. Although the option to use 4-layer air traffic and humidity data appeared to affect the results in the west more than in the eastern CONUS (which may be the consequence of the relatively smaller amounts of air traffic over the western USA), the increased vertical resolution did not improve the results of the simulations when compared to the satellite retrievals. The failure of the 4-layer option to improve the contrail coverage simulations suggests that most contrails detected by the satellite either develop in relatively deep layers of high humidity, or that the RUC model has a limited ability to diagnose the

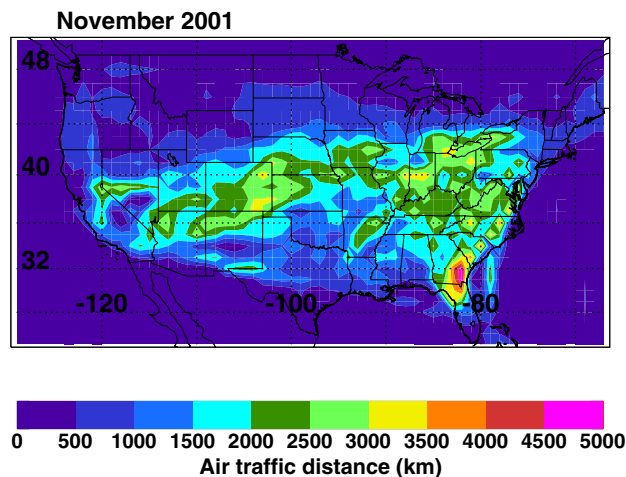


**Figure 7:** Mean air traffic density (flight distance (km)/ $1^{\circ} \times 1^{\circ}$  grid box/hour) computed for November 2001. The air traffic density field for September 2001 (not shown) is similar.

vertical structure of upper tropospheric humidity accurately.

The simulations with cloud masks produced similar results and yielded greater RMS differences overall than the simulations that used no cloud mask. It appears likely that no cloud mask is necessary for the simulations, and that the contrail detection algorithm is not significantly affected by underlying cloudiness. Indeed, contrails are often detected in both thin and thick cirrus clouds (e.g., PALIKONDA et al., 2005).

Some of the differences between the simulated and satellite-derived coverage is surely attributable to errors in the satellite retrieval. Although thick clouds may obscure some of the observed coverage, the objective retrieval can also overestimate contrail coverage in cloudy areas because it identifies cloud streets and cirrus streamers as contrails (e.g., MINNIS et al., 2005A). A manual analysis of randomly selected results from 2 months of the CONUS satellite analyses (PALIKONDA et al., 2005) indicated that the objective contrail detection algorithm missed an additional 5 and 10 % of contrails. However, nearly 50–60 % of all pixels identified as contrails were judged to be other cloud features such as cumulus cloud streets and cirrus streamers for those two months (April and July 2001). The greatest overestimates occurred over Canada and outlying ocean areas suggesting that the errors were smaller over the CONUS. Better regional and overall quantification of the satellite errors are needed to fully assess how much of the RMS difference in Table 1 is due to the satellite observations.

More satellite data must also be analyzed and additional model simulations are needed to help understand interannual and diurnal variability in both PCF and contrail coverage. The results from PALIKONDA et al. (2005) were taken during 2001 when the upper troposphere over the CONUS was unusually dry.

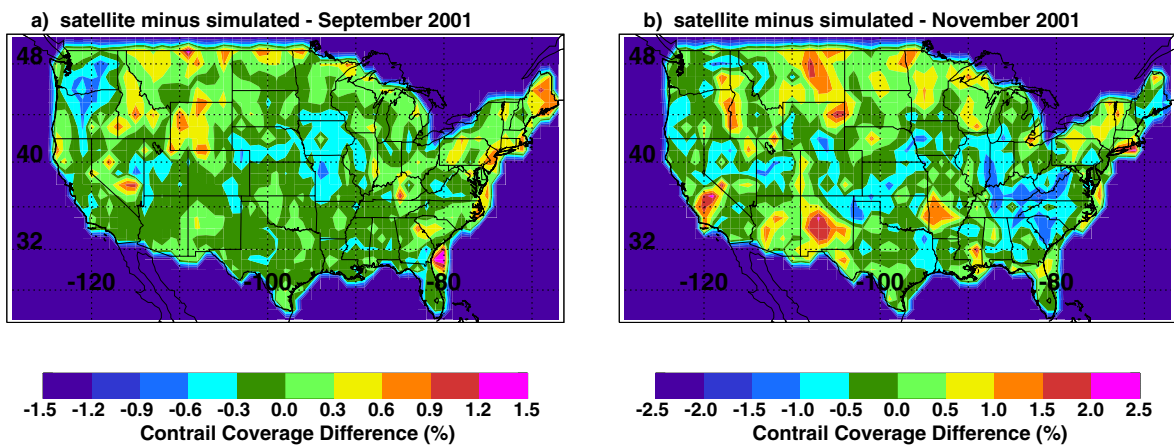


**Figure 8:** (a) Satellite-derived minus scenario D6 simulated contrail coverage for September 2001. (b) Same as (a), but for November 2001.

Additionally, the initial comparisons of the NOAA-15 and NOAA-16 contrail coverage estimates from 2001 (PALIKONDA et al., 2005) suggest that the relationship between detectable contrails and air traffic might vary with time of day because of saturation effects. That is, more contrails form in the morning when the upper troposphere is cleaner and has been crossed by relatively few airplanes during the previous 6 hours. During the afternoon, the air that was susceptible to contrail formation early in the morning has either been saturated with contrails and their antecedent cirrus clouds to some extent by the hours of passing air traffic or the excess moisture in the relevant altitudes has been reduced significantly by precipitation of the contrail ice crystals formed earlier in the day. The results from other satellite platforms such as NOAA-15 and the NASA Terra, with crossover times approximately 7 and 4 hours before NOAA-16, would help determine whether the relationship between contrail coverage and air traffic truly changes throughout the day. That type of variation would need to be included in any future simulation. Simulations of other months of data will also help to determine the cause of the regional differences between the observed and simulated coverages during the two months presented above.

To improve the simulated coverages, more comparisons are needed between satellite-based estimates of contrail coverage and the PCFs diagnosed from RUC analyses and other numerical weather analyses. Numerical weather prediction models are not designed with an emphasis on accurate upper tropospheric humidity. Although an improvement over radiosonde measurements in terms of temporal and spatial coverage, models such as the RUC still have a dry bias in relative humidity in the upper troposphere. The use of a temperature-dependent RHI threshold appeared to improve the comparison between the simulated and observed coverages. Significant changes in the model physics as seen in the RUC20 results (Figure 1) profoundly affect the computation of PCF and must be considered in future studies.

Most ice supersaturations have been eliminated from the current RUC20 analyses, and new schemes to relate persistent contrail formation to the meteorological variables must be developed. Comparisons of RUC-based PCFs with contrail observations will help in the development of these schemes, and to determine areas where the RUC has difficulties in analyzing relative humidity. To accommodate the occasional changes in the RUC model, a statistics-based method similar to model output statistics (MOS) (GLAHN and LOWRY, 1972) could be used in future contrail simulation models. Meanwhile, other numerical weather analysis results should be tested in this simulation scheme to determine if they can provide any better accuracy than found with the RUC results.

Two factors not addressed here but implied from the results presented above may have important effects on contrail coverage. The differences between the observed and simulated coverages over the Great Plains (approximately 40°N, 100°W) suggest that the effects of synoptic-scale vertical motions may be important to the development of contrails and must be included in future studies. Contrail advection has also not been considered, and may account for the larger observed coverages off the eastern coast of the CONUS as contrails advect from a large area of high traffic density to the Atlantic.

## 6 Summary and concluding remarks

A new estimate of the line-shaped contrail coverage over the contiguous United States of America was computed by combining for the first time hourly temperature and humidity analyses from an operational numerical weather prediction model with actual commercial air travel statistics. Potential contrail frequencies (PCF) were computed directly from the meteorological data using classical contrail formation criteria. PCFs computed for two months (September and November 2001) show large variations in magnitude depending on the synoptic-scale pattern. The distribution of PCFs computed during NOAA-16 overpasses suggest that potential contrail

frequency is not strongly influenced by the time of the satellite observation.

Several scenarios of simulated contrail coverage were computed for both months using several model options. The simulated coverage was compared to satellite-derived contrail coverage estimates from NOAA-16 AVHRR measurements. For the simplest diagnosis scheme, scenario A, the simulated persistent contrail coverage was heavily influenced by the air traffic pattern, similar to earlier studies. The small magnitude of the  $c_{fl}$  parameter reveals that even in areas suitable for contrail formation, only a small fraction of all flights produce persistent contrails that are detectable by satellite. The contrail coverage computed from NOAA-16 imagery, however, was more closely related to the potential contrail frequency (and high cloud coverage) than to air traffic density. This suggests that the coverage of line-shaped contrails is non-linearly related to air traffic, and “saturation” effects are important in high traffic areas.

Several factors were tested to determine their effects on the simulation of contrail coverage, and the scenario most closely matching the satellite retrievals was scenario D6, which used the temperature-dependent RHI threshold to account for the overall dry bias in the RUC analyses and the fourth-root relationship with air traffic. Some of the most notable differences between scenario D6 and the satellite-derived coverage occurred in regions with significant military air traffic that is not included in the air traffic database, as well as areas where cloud streets and cirrus contamination are likely. Increasing the vertical resolution of the air traffic and humidity data did not appear to improve the results of the simulations significantly in comparison with the satellite retrievals of contrail coverage.

Although the simulations in scenario D6 produced a better match with the satellite retrievals than the simple simulations in scenario A, more work remains to determine how much of the contrail coverage pattern is influenced by the air traffic density versus the upper tropospheric conditions reflected in the PCF. Sensitivity to other factors including aircraft type (engine efficiency) and numerical weather analysis source should also be tested. It is likely that the differences between simulated and observed contrail coverage will be reduced further using the suggested tests and improvements described in Section 5.

The framework developed here for simulating contrails in a realistic fashion will be extremely valuable not only for diagnosing linear contrail formation but also for examining parameterizations of contrail spreading and contrail optical properties, parameters necessary for determining and predicting contrail climate effects. By comparisons with the observed contrails, the simulations should be useful for providing data needed to model the rate of persistent contrail spreading, and to correct

biases in upper tropospheric humidity, a variable that could ultimately improve weather forecasts. Because the methodology described in this study is based on hourly numerical weather analyses, it is possible to apply it in near-real time or in a forecast mode using predictions instead of analyses. If operated in a predictive fashion, it would be possible to confidently prognosticate those altitudes and areas where contrail outbreaks are likely. With such information, it should be possible for air traffic controllers to reroute some of the upcoming flights to avoid the areas of potential contrail coverage and mitigate some of the potential climate impacts of air travel while conserving fuel in areas when contrail formation potential is low. Much additional research is required, however, to reach the level of confidence needed for implementation of a contrail prediction scheme, an act that would certainly disrupt many aspects of the present air traffic system. Nevertheless, the prototype contrail diagnosis model presented in this study represents an important step in developing accurate contrail forecasts and the effects of contrails on climate.

## Acknowledgements

This research was supported by grants NASA NAG-1-2135 and NAG-1-02044, the NASA Pathfinder Program and the NASA Radiation Sciences Program. The authors wish to thank Yan CHEN for providing the ice cloud coverage figures.

## References

- ALDUCHOV, O. A., R. E. ESKRIDGE, 1996: Improved Magnus form approximation of saturation vapor pressure. - *J. Appl. Meteor.* **35**, 601–609.
- APPLEMAN, H., 1953: The formation of exhaust condensation trails by jet aircraft. - *Bull. Amer. Meteor. Soc.* **34**, 14–20.
- BAKAN, S., M. BETANCOR, V. GAYLER, H. GRASSL, 1994: Contrail frequency over Europe from NOAA-satellite images. - *Ann. Geophys.* **12**, 962–968.
- BARNES, W. L., T. S. PAGANO, V. V. SALOMONSON, 1998: Prelaunch characteristics of the Moderate Resolution Imaging Spectroradiometer (MODIS) on EOS-AM1. *IEEE Trans. Geosci. Remote Sens.* **36**, 1088–1100.
- BENJAMIN, S. G., J. M. BROWN, K. J. BRUNDAGE, D. DÉVÉNYI, G. A. GRELL, D. KIM, B. E. SCHWARTZ, T. G. SMIRNOVA, T. L. SMITH, S. S. WEYGANDT, G. S. MANIKIN, 2004: An hourly assimilation/forecast cycle: The RUC. - *Mon. Wea. Rev.* **132**, 495–518.
- BJORNSON, B. M., 1992: SAC contrail formation study. - USAFETAC/PR-92/003, USAF Environmental Technical Applications Center, Scott Air Force Base, Illinois 62225-5438.
- BOUCHER, O., 1999: Air traffic may increase cirrus cloudiness. - *Nature* **397**, 30–31.
- BUSEN, R., U. SCHUMANN, 1995: Visible contrail formation from fuels with different sulfur contents. - *Geophys. Res. Lett.* **22**, 1357–1360.

- DUDA, D. P., P. MINNIS, L. NGUYEN, R. PALIKONDA, 2004: A case study of the development of contrail clusters over the Great Lakes. – *J. Atmos. Sci.* **61**, 1132–1146.
- GARBER, D. P., P. MINNIS, K. P. COSTULIS, 2005: A commercial flight track database for upper tropospheric aircraft emission studies over the USA and southern Canada. – *Meteorol. Z.* **14**, 445–452.
- GLAHN, H. R., D. A. LOWRY, 1972: The use of model output statistics (MOS) in objective weather forecasting. – *J. Appl. Meteor.* **11**, 1203–1211.
- MANNSTEIN, H., R. MEYER, P. WENDLING, 1999: Operational detection of contrails from NOAA-AVHRR data. – *Int. J. Remote Sensing* **20**, 1641–1660.
- MARQUART, S., B. MAYER, 2002: Towards a reliable GCM estimation of contrail radiative forcing. – *Geophys. Res. Lett.* **29**(8), DOI:10.1029/2001GL014075.
- MARQUART, S., M. PONATER, F. MAGER, R. SAUSEN, 2003: Future development of contrail cover, optical depth and radiative forcing: Impacts of increasing air traffic and climate change. – *J. Climate* **16**, 2890–2904.
- MEYER, R., H. MANNSTEIN, R. MEERKÖTTER, U. SCHUMANN, P. WENDLING, 2002: Regional radiative forcing by line-shaped contrails derived from satellite data. – *J. Geophys. Res.* **107**, 10.1029/2001JD000426.
- MILOSHEVICH, L. M., H. VÖMEL, A. PAUKKUNEN, A. J. HEYMSFIELD, S. J. OLTMANS, 2001: Characterization and correction of relative humidity measurements from Vaisala RS80-A radiosondes at cold temperatures. – *J. Atmos. Oceanic Technol.* **18**, 135–156.
- MINNIS, P., D. F. YOUNG, D. P. GARBER, L. NGUYEN, W. L. SMITH, JR, R. PALIKONDA, 1998: Transformation of contrails into cirrus during SUCCESS. – *Geophys. Res. Lett.* **25**, 1157–1160.
- MINNIS, P., U. SCHUMANN, D. R. DOELLING, K. M. GIERENS, D. W. FAHEY, 1999: Global distribution of contrail radiative forcing. – *Geophys. Res. Lett.* **26**, 1853–1856.
- MINNIS, P., D. F. YOUNG, B. A. WIELICKI, D. P. KRATZ, P. W. HECK, S. SUN-MACK, Q. Z. TREPTE, Y. CHEN, S. L. GIBSON, R. R. BROWN, 2002: Seasonal and diurnal variations of cloud properties derived for CERES from VIRS and MODIS data. – Proc. 11th Conf. Atmospheric Radiation, Ogden, Utah, Amer. Meteor. Soc., Boston, 20–23.
- MINNIS, P., J. K. AYERS, R. PALIKONDA, D. PHAN, 2004: Contrails, cirrus trends, and climate. – *J. Climate* **17**, 1671–1685.
- MINNIS, P., R. PALIKONDA, B. J. WALTER, J. K. AYERS, H. MANNSTEIN, 2005A: Contrail properties over the eastern North Pacific from AVHRR data. – *Meteorol. Z.* **14**, 513–521.
- MINNIS, P., Y. YI, J. HUANG, J. K. AYERS, 2005B: Relationships between radiosonde and RUC-2 meteorological conditions and cloud properties determined from ARM data. – *J. Geophys. Res.* 10.1029/2005JD006005, submitted.
- MYHRE, G., F. STORDAL, 2001: On the tradeoff of the solar and thermal infrared radiative impact of contrails. – *Geophys. Res. Lett.* **28**, 3119–3122.
- PALIKONDA, R., P. MINNIS, D. R. DOELLING, P. W. HECK, D. P. DUDA, H. MANNSTEIN, U. SCHUMANN, 1999: Potential radiative impact of contrail coverage over continental USA estimated from AVHRR data. – Proc. 10th Conf. Atmospheric Radiation, Madison, Wisconsin. Amer. Meteor. Soc. Boston, 181–184.
- PALIKONDA, R., P. MINNIS, D. P. DUDA, H. MANNSTEIN, 2005: Contrail coverage derived from 2001 AVHRR data over the continental United States of America and surrounding areas. – *Meteorol. Z.* **14**, 525–536.
- PONATER, M., S. MARQUART, R. SAUSEN, 2002: Contrails in a comprehensive global climate model: Parameterization and radiative forcing results. – *J. Geophys. Res.* **107**, 10.1029/2001JD000429.
- SAUSEN, R., K. GIERENS, M. PONATER, U. SCHUMANN, 1998: A diagnostic study of the global distribution of contrails. Part I: Present day climate. – *Theor. Appl. Climatol.* **61**, 127–141.
- SCHRADER, M. L., 1997: Calculations of aircraft contrail formation critical temperatures. – *J. Appl. Meteor.* **36**, 1725–1729.